Title

Reentrant phase behavior and coexistence in asymmetric block copolymer electrolytes

Journal

Soft Matter, 14(15)

ISSN

1744-683X

Authors

Loo, Whitney S

Jiang, Xi

Maslyn, Jacqueline A

et al.

Publication Date

2018-04-18

DOI

10.1039/c8sm00175h

Peer reviewed

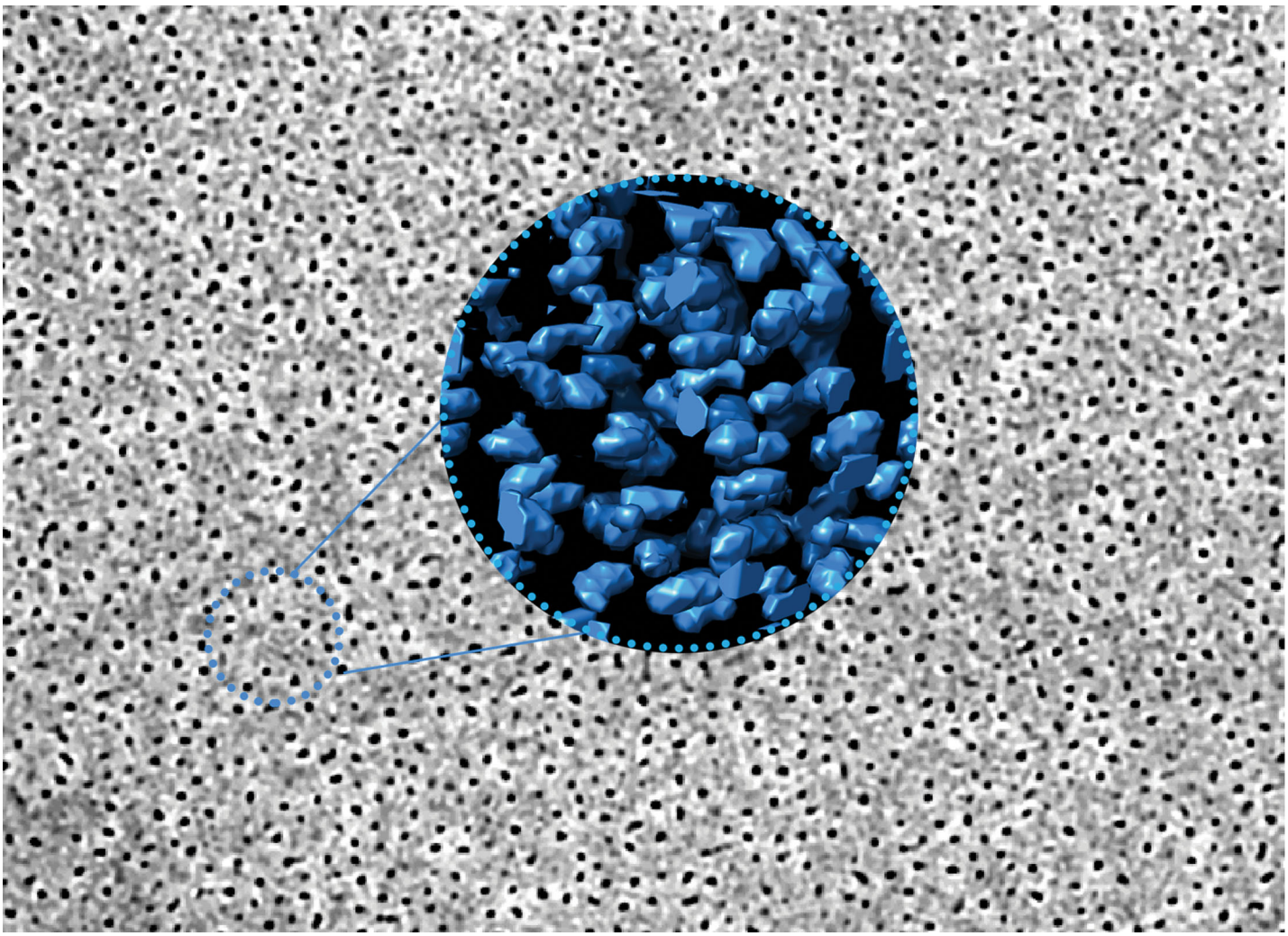

Highlighting research from the University of California, Berkeley, from the group of Nitash P. Balsara.

Reentrant phase behavior and coexistence in asymmetric block copolymer electrolytes

Loo *et al*. report the coexistence of two ordered morphologies of a single lattice type in a salt-containing diblock copolymer system through electron tomography and small angle X-ray scattering. The two self-assembled body center cubic lattices are found to be in equilibrium with each other.

As featured in:

See Nitash P. Balsara *et al.*, *Soft Matter*, 2018, **14**, 2789.

ROYAL SOCIETY OF CHEMISTRY

rsc.li/soft-matter-journal

Registered charity number: 207890

Soft Matter

PAPER

View Article Online
View Journal | View Issue

Cite this: *Soft Matter*, 2018, **14**, 2789

Reentrant phase behavior and coexistence in asymmetric block copolymer electrolytes†

Whitney S. Loo,[a] Xi Jiang,[b] Jacqueline A. Maslyn,[ab] Hee Jeung Oh,[a] Chenhui Zhu,[c] Kenneth H. Downing[d] and Nitash P. Balsara*[abe]

Received 24th January 2018,
Accepted 28th February 2018

DOI: 10.1039/c8sm00175h

rsc.li/soft-matter-journal

It is known that the addition of salts to symmetric block copolymers leads to stabilization of ordered phases and an increase in domain spacing; both trends are consistent with an increase in the effective Flory–Huggins interaction parameter between the blocks, χ. In this work, we show that the addition of salt to a disordered asymmetric block copolymer first leads to the formation of coexisting ordered phases which give way to a reentrant disordered phase at a higher salt concentration. The coexisting phases are both body centered cubic (BCC) with different domain spacings, stabilized by partitioning of the salt. Further increase in salt concentration results in yet another disorder-to-order transition; hexagonally packed cylinders are obtained in the high salt concentration limit. The coexisting phases formed at intermediate salt concentration, elucidated by electron tomography, showed the absence of macroscopic regions with distinct BCC lattices. A different asymmetric block copolymer with composition in the vicinity of the sample described above only showed only a single disorder-to-order transition. However, the dependence of domain spacing on salt concentration was distinctly non-monotonic, and similar to that of the sample with the reentrant phase behavior. This dependence appears to be an announcement of reentrant phase transitions in asymmetric block copolymer electrolytes. These results cannot be mapped on to the traditional theory of block copolymer electrolyte self-assembly based on an effective χ.

Introduction

There is continuing experimental[1–8] and theoretical[9–12] interest in the thermodynamic properties of block copolymer electrolytes. A commonly studied system is polystyrene-*block*-poly(ethylene oxide) (SEO) mixed with lithium bis(trifluoromethanesulfonyl) imide salt, SEO/LiTFSI. The thermodynamic interactions in these systems are often expressed in terms of an effective Flory-Huggins interaction parameter between the blocks, χ. Current work suggests that χ increases with increasing salt concentration.[2–5,13,14] It is, perhaps, surprising that the addition of salt to disordered block copolymers generally results in the formation of ordered phases.[15–17] Experimental work thus far focuses on symmetric (or nearly symmetric) block copolymers.[2,18,19] The purpose of this paper is to describe the thermodynamic properties of a series of asymmetric block copolymer electrolytes. Our work builds on previous studies on neat asymmetric block copolymers.[20–22] Particularly relevant to the present study is the limited long-range order observed in some asymmetric systems.[23–25] We report on disorder–order and order–order phase transitions that are very different from those reported in previous studies. In particular, we show that reentrant phase transitions are possible in these systems. The addition of salt to a disordered block copolymer first leads to the formation of ordered phases which give way to a reentrant disordered phase upon further salt addition. In the ordered state, we find two coexisting phases with the same geometry but different lattice constants.

Experimental section

Synthesis and preparation of the block copolymer electrolytes

The SEO copolymers were synthesized using methods described in ref. 26 and purified using methods described in ref. 4. The electrolytes were prepared according to methods described in ref. 27 using argon gloveboxes. SAXS samples were

[a] *Department of Chemical and Biomolecular Engineering, University of California-Berkeley, Berkeley, California 94720, USA. E-mail: nbalsara@berkeley.edu*
[b] *Materials Sciences Division, Lawrence Berkeley National Laboratory, Berkeley, California 94720, USA*
[c] *Advanced Light Source, Lawrence Berkeley National Laboratory, Berkeley, California 94720, USA*
[d] *Molecular Biophysics and Integrated Bioimaging Division, Lawrence Berkeley National Laboratory, Berkeley, California 94720, USA*
[e] *Energy Technologies Division, Lawrence Berkeley National Laboratory, Berkeley, California 94720, USA*

† Electronic supplementary information (ESI) available. See DOI: 10.1039/c8sm00175h

prepared by pressing/melting the polymer into a 1/8 in. diameter spacer made of 1/32 in. thick Aflas rubber and annealing them at 120 °C overnight followed by a 24 hour period of controlled cooling under vacuum to room temperature. The samples were sealed with Kapton windows.

Small angle X-ray scattering (SAXS)

SAXS measurements were performed at beamline 7.3.3. at the Advanced Light Source (ALS) at Lawrence Berkeley National Laboratory[28] and beamline 1–5 at the Stanford Synchrotron Radiation Lightsource (SSRL) at SLAC National Accelerator Laboratory. Silver behenate was used to determine the beam center and sample-to-detector distance. The scattered intensity was corrected for beam transmission and empty cell scattering. Two-dimensional scattering patterns were integrated azimuthally using the Nika program for IGOR Pro to produce one-dimensional scattering profiles and are reported as scattering intensity, I, as a function of the scattering vector, q.[29] Measurements were taken in a custom-built 8-sample heating stage, starting at 132 °C and cooling in steps of about 10 °C to 75 °C. Samples were annealed for about 30 min at each temperature before taking measurements. A typical temperature scan takes about six hours (including time required to cool the sample stage). To a good approximation, the SAXS profiles of all our samples were independent of temperature in the range studied. We thus only discuss data obtained at the highest temperature in the main text. The temperature range of our SAXS experiments is well above the melting temperature of the crystallizable poly(ethylene oxide) (PEO) block. Data obtained at the lowest temperature, 75 °C, is shown in the ESI.†

Electron tomography

A bulk sample, annealed using the same protocol used to prepare the SAXS samples, was sectioned at −120 °C using cryo-microtome (Leica Ultracut 6) to obtain an ultrathin film (~100 nm). The ultrathin film was transferred to C-flat grid with ultrathin continuous carbon supporting film and stored in a glove box immediately after cryo-microtoming to minimize the effect of humidity. PEO domains were stained to increase contrast and stability under electron beam by exposing the ultrathin film to RuO_4 vapor for 10 minutes at room temperature. 5 nm gold colloid nanoparticles were deposited on the backside of the grid as fiducial markers. Dual-axis tomography was performed using Philps CM200 transmission electron microscope at 200 KV at the Donner Lab Electron Microscopy Facility at Lawrence Berkeley National Lab. The tilt series were collected with 1.5 degrees step from −65 to 65 degrees. Tomograms were reconstructed and filtered (nonlinear anisotropic diffusion filter) in IMOD. The tomogram of a small area was binarized for segmentation by adjusting threshold.[30–32]

Results and discussion

The properties of the polymers used in this study are given in Table 1. We refer to each copolymer by its molecular weight, for example, in SEO(9.4–4.0) the molecular weights of the polystyrene (PS) and PEO blocks are 9.4 kg mol^{-1} and 4.0 kg mol^{-1}. Fig. 1 shows the scattering profiles of the block copolymer electrolytes at 132 °C at selected salt concentrations. LiTFSI concentrations are reported as the molar ratio of lithium ions to ethylene oxide moieties: $r = \frac{[\mathrm{Li}]}{[\mathrm{EO}]}$. For SEO(9.4–4.0), Fig. 1a, we see that the addition of salt drives microphase separation, as previously reported.[4,5,7] The broad scattering peak obtained in the neat sample becomes sharper at r = 0.005. The scattering profiles obtained in this salt concentration regime ($0 \leq r \leq 0.005$) are consistent with a disordered state. Further increase of salt concentration to r = 0.01 results in dramatic sharpening of the primary scattering peak and the emergence of higher order scattering reflections at $\frac{q}{q^*} = \sqrt{3}$ and $\sqrt{4}$ where q^* is the location of the primary scattering peak, consistent with a hexagonally packed cylindrical phase (HEX). These reflections persist at all remaining salt concentrations, and at higher salt concentrations, $r \geq 0.025$, higher order reflections at $\frac{q}{q^*} = \sqrt{7}$ and $\sqrt{9}$ appear. For SEO(17.4–3.9), Fig. 1b, the neat sample is also disordered, and the addition of salt induces microphase separation at all measured salt concentrations ($0.005 \leq r \leq 0.075$). The higher order scattering reflections in this sample are located at $\frac{q}{q^*} = \sqrt{2}, \sqrt{3}$ and $\sqrt{6}$ indicative of a body center cubic spherical phase (BCC). The $\frac{q}{q^*} = \sqrt{2}$ peak is not detected for r = 0.01, 0.05, and 0.075 due to the broadening of the primary q^* peak.

Table 1 Characteristics of polymers synthesized and used in this study

Polymer	M_{PS} (kg mol^{-1})	M_{PEO} (kg mol^{-1})	f_{EO}	PDI	N_{PS}	N_{EO}	N
SEO(17.4–3.9)	17.4	3.9	0.18	1.04	287	63	350
SEO(9.4–2.4)	9.4	2.4	0.20	1.04	155	39	194
SEO(9.4–4.0)	9.4	4.0	0.29	1.04	155	65	220

Parameters f_{EO}, N_{PS}, N_{EO} were evaluated at 140 °C

More complex phase transformations are seen with SEO(9.4–2.4), Fig. 1c. The neat polymer is disordered as is the mixture with r = 0.005. However, we see the emergence of two coexisting BCC phases at r = 0.01. The scattering signatures of the larger BCC lattice are indicated by open symbols while those of the smaller BCC lattice are indicated by filled symbols in Fig. 1c. Reflections at $\frac{q}{q^*} = \sqrt{2}$ and $\sqrt{3}$ corresponding to both lattices are seen in Fig. 1c. To our knowledge, two coexisting lattices with the same symmetry have been neither observed nor predicted in block copolymer systems. The domain spacing, given by $d = \frac{2\pi}{q^*}$, of the two coexisting BCC lattices are 12.8 and 14.8 nm. It is apparent that the two BCC phases must have different salt concentrations; if this were not the case, it is impossible to rationalize the presence of two coexisting morphologies.[33] Further increase in overall salt concentration to r = 0.025 results in the formation of a reentrant disordered phase. Finally, at r = 0.05 and r = 0.075, a single HEX phase is

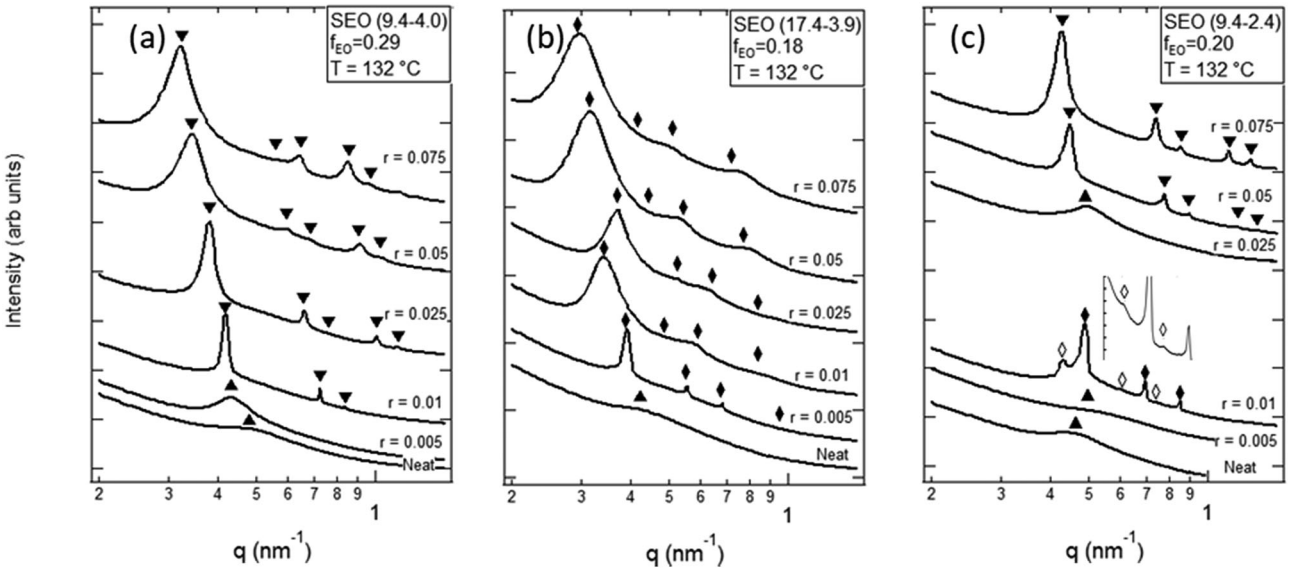

Fig. 1 SAXS profiles at 132 °C for (a) SEO(9.4–4.0) (b) SEO(17.4–3.9) and (c) SEO(9.4–2.4) at varying salt concentrations. The ▲, ▼, ♦ represent primary and higher ordering scattering peaks for morphologies DIS, HEX, BCC respectively. The presence of both filled and open symbols indicates coexistence between ordered phases.

obtained with higher order scattering reflections at $\frac{q}{q^*} = \sqrt{3}, \sqrt{4}, \sqrt{7}$ and $\sqrt{9}$. SEO(9.4–2.4) exhibits phase behavior that appears to be a combination of behaviors observed in SEO(9.4–4.0) and SEO(17.4–3.9). While SEO(9.4–4.0) and SEO(17.4–3.9) electrolytes exhibit HEX and BCC phases in the ordered state, SEO(9.4–2.4) electrolytes exhibit both ordered phases. For all three block copolymers, the addition of salt results in broadening of SAXS peaks associated with the ordered phase, suggesting a decrease in long-range order. In previous studies, we have used TEM to establish this effect, which arises due to the formation of temporary crosslinks created by the coordination of PEO chains and Li^+ ions that impede chain motion.[34]

The disordered and ordered morphologies of the block copolymer electrolytes are shown in Fig. 2a on a plot of salt concentration in the PEO domains, r, versus volume fraction of the PEO-rich domains, $f_{EO,salt}$. We calculate $f_{EO,salt}$ based on the assumption that LiTFSI preferentially segregates into the PEO domains and from reported densities of LiTFSI/PEO mixtures in ref. 35.[36,37] The phase diagram contains three sets of data points representing the three polymers; as salt is added to the copolymer, $f_{EO,salt}$ increases linearly with r for each polymer. SEO(9.4–4.0) and SEO(17.4–3.9) exhibit one salt-induced phase transformation from DIS to HEX and DIS to BCC respectively. SEO(9.4–2.4) exhibits three phase transformations: DIS to coexisting BCC lattices to DIS to HEX. The Gibbs phase rule requires coexistence at all phase boundaries. We conclude that the widths of all of the coexistence windows in the samples are smaller than our coarse steps in salt concentration; for example, the Gibbs phase rule necessitates coexistence of DIS and BCC phases at the disorder–order boundary.[16] The origin of the two coexisting BCC lattices, which were observed throughout the entire temperature window in two independently prepared samples, is not clear. Fig. 2a thus applies to the entire temperature window. The fact that the morphologies of the copolymers listed in Table 1 can be represented on a simple r versus $f_{EO,salt}$ diagram (Fig. 2a) is non-trivial.

The effect of added salt on block copolymer thermodynamics is due to two competing factors: (1) the addition of salt generally increases the effective χ between the blocks and induces ordering, (2) the salt molecules partition into and swell the PEO domains, thereby increasing f_{EO}. The f_{EO} of neat SEO(9.4–2.4) is 0.20, which is at the border between BCC and HEX phases. (Floudas *et al.* studied the phase behavior of poly(ethylene oxide)-*block*-polyisoprene block copolymers, where the BCC/HEX border was identified at f_{EO} = 0.21.[22]) Adding salt to SEO(9.4–2.4) at r = 0.01 results in the formation of coexisting BCC lattices consistent with (1). The salt concentration at this composition does not result in sufficient swelling of the PEO domain to obtain hexagonally packed PEO cylinders. This phase is only formed at $r \geq 0.05$. The disordered phase at an intermediate salt concentration, r = 0.025, is due to the interplay between the two competing factors.

The dependence of domain spacing, d, on salt concentration, r, is shown in Fig. 2b. The colors in the figure depict the morphology of the electrolytes. The simplest behavior is seen in SEO(9.4–4.0) wherein d increases monotonically with increasing r with no discontinuity at the DIS to HEX transition.[2–4] The domain spacing of neat SEO(9.4–2.4) is identical to that of neat SEO(9.4–4.0), but it decreases with increasing salt concentration before increasing at r = 0.01 where two coexisting BCC lattices are obtained. It is unusual that a salt-containing sample would have a lower d compared to its neat counterpart. Further increase of salt concentration results in a decrease in d as the sample disorders. At $r \geq 0.025$, d increases

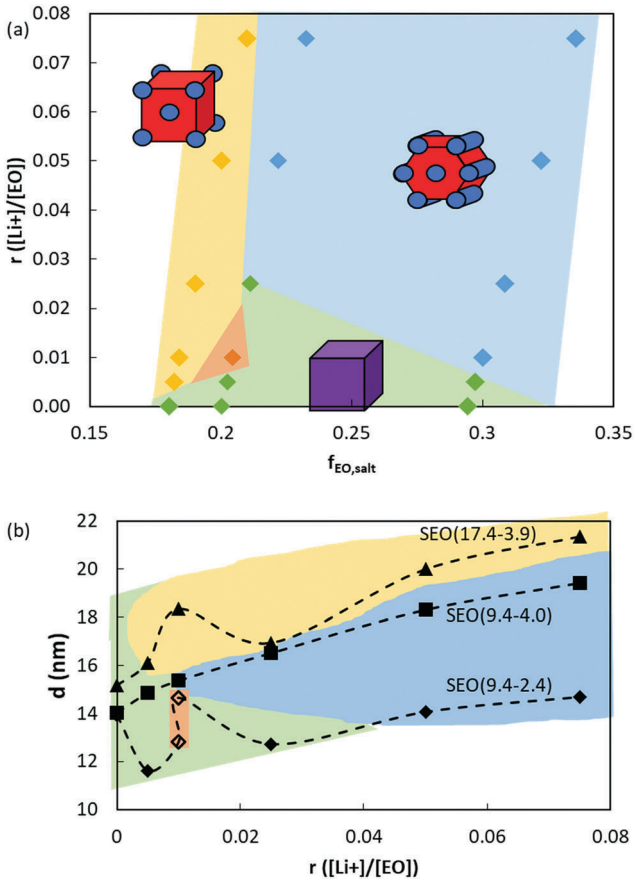

Fig. 2 (a) Phase behavior of SEO/salt mixtures on a plot of salt concentration versus volume fraction of the PEO-rich conducting microphase at 75 –132 °C (b) domain spacing of a series of SEO block copolymers at 132 °C as a function of salt concentration. For both diagrams, the yellow, blue, green and orange regions correspond to BCC, HEX, DIS, and coexisting BCC phases, respectively.

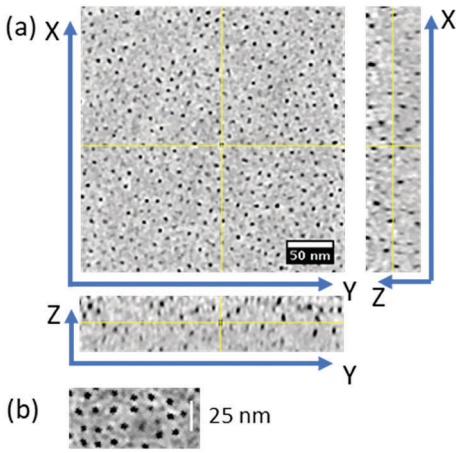

Fig. 3 (a) Tomogram obtained from dual-axis reconstruction of RuO_4 stained SEO/LiTFSI r = 0.01 sample. Dark domains represent the RuO_4 stained PEO block. (b) Region of tomogram with increased long-range order. Scale bar represents 25 nm.

monotonically with increasing r with no discontinuity at the DIS to HEX transition. The dependence of d on r of SEO(17.4–3.9) is most interesting. This sample exhibits a simple DIS to BCC transition, but the dependence of d on r is non-monotonic, similar to that of SEO(9.4–2.4). These two copolymers have similar compositions but their chains lengths differ by a factor of 1.8. One may thus regard the non-monotonic dependence of d on r in SEO(17.4–3.9) as "announcements" of BCC coexistence at lower molecular weights in the same composition window.

The chains of SEO(9.4–2.4) at r = 0.01 exhibit different extents of chain stretching, depending on the BCC lattice they belong to. The reason for the fact that the coexisting morphology has a lower free energy than that of a single BCC phase with intermediate chain stretching remains to be determined. Computer simulations suggest that each lithium ion is associated with six coordinating oxygen atoms.[38–40] Perhaps, discrete chain conformations are preferred due to these interactions, and the free energy gain from adopting these conformations is large enough to offset the entropic penalty of heterogeneous salt distribution.

The nature of the coexisting BCC lattices was further studied by transmission electron tomography. We are not aware of any prior studies wherein electron tomography has been used to study the morphology of weakly ordered block copolymers in the vicinity of order–disorder transitions. Three dimensional tomograms were obtained from the r = 0.01 sample of SEO(9.4–2.4)/LiTFSI stained with RuO_4. Fig. 3a shows slices of the tomogram obtained from dual-axis reconstruction of the data. The dark domains represent the RuO_4 stained PEO/LiTFSI spherical domains. Electron tomography confirms that the sample contains only spheres, consistent with our interpretation of the SAXS profile. It is also evident, however, that our sample does not contain easily identifiable macroscopic regions with two different lattice constants. Some regions did, however, show evidence of BCC lattices with limited long-range order. One such region is shown in Fig. 3b. Quantitative analysis of the entire tomogram is necessary to reveal correlations between the spherical domains.

Fig. 4a shows the Fourier transform (FT) of a typical slice obtained by electron tomography; *e.g.* see Fig. 3a. The anisotropy of the FT is attributed to distortion due to compression along one axis during cryo-sectioning. Fig. 4b shows a sector-averaged intensity versus scattering vector, q, for the FT. The averaging was conducted along the non-compressed axis, indicated by the white arrow in Fig. 4a. The circularly averaged FT of the same slice, shown by a continuous black line in Fig. 4b is qualitatively similar to the sector-averaged FT. The FT analysis was repeated for several slices and the results of three slices are given in the ESI† (Fig. S2). All of the FTs are very similar to that given in Fig. 4b. The arrows in Fig. 4b indicate the positions of the primary peaks observed in SAXS; recall that SAXS revealed the presence of two BCC lattices. There is reasonable agreement between the FT peak and the SAXS data. The relatively subtle difference in the lattice constants of the coexisting BCC structures obtained by SAXS are lost in the FT analysis. We posit that this is due to complications related to the electron tomography experiments such as missing spheres due to incomplete staining and distortions during cryo-sectioning. While our TEM data provide support for our interpretation of

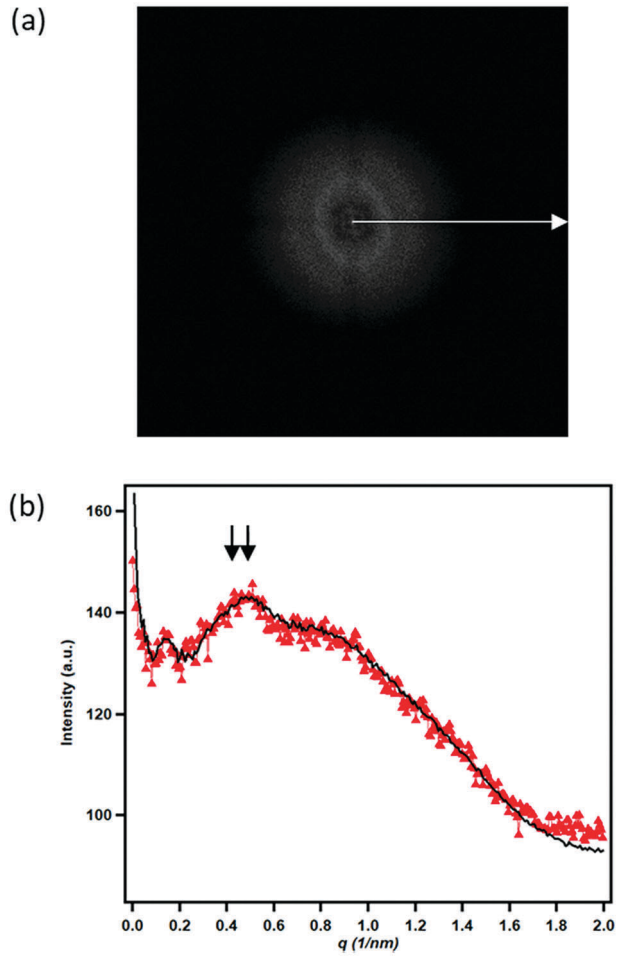

Fig. 4 (a) FT of single slice of tomogram. Sector average was performed along the white arrow. (b) Sector averaged (red triangles) and circular averaged (black line) intensity versus scattering vector, q. The black arrows indicate the locations of the observed primary SAXS peaks.

the SAXS profile of SEO(9.4–2.4) r = 0.01, it also reveals the complexity of coexisting phases that are obtained in the vicinity of order–disorder transitions.

Conclusion

In conclusion, we have determined the morphology of mixtures of asymmetric block copolymers and a lithium salt by SAXS and electron tomography. SAXS results show that the addition of salt to a disordered asymmetric block copolymer first leads to the formation of coexisting BCC lattices, which give way to a reentrant disordered phase at a higher salt concentration. Further increase in salt concentration results in the formation of hexagonally packed cylinders. Electron tomography showed the absence of macroscopic regions with distinct BCC lattices. However, the Fourier transforms of tomogram slices were qualitatively consistent with the SAXS results. Doubling the chain length at fixed composition (or nearly so) resulted in a single disorder-to-order transition with added salt. Reducing the asymmetry at fixed chain length (or nearly so) also resulted in a single disorder-to-order transition with added salt. These results cannot be mapped on to any of the existing theories of the thermodynamics of block copolymer/salt mixtures.[9–12]

Author contributions

The manuscript was written through contributions of all authors. All authors have given approval to the final version of the manuscript.

Funding sources

W. S. L acknowledges funding from National Science Foundation Graduate Student Research Fellowship DGE-1106400.

Conflicts of interest

The authors declare no competing financial interest.

Acknowledgements

Primary funding for this work was provided by the National Science Foundation through Award DMR-1505444. Funding for the electron tomography work was provided by the Soft Matter Electron Microscopy Program, supported by the Office of Science, Office of Basic Energy Science, US Department of Energy, under Contract DE-AC02-05CH11231. Work at the Donner Lab and the Advanced Light Advanced Light Source, which is a DOE Office of Science User Facility, was supported by contract no. DE-AC02-05CH11231. Work at the Stanford Synchrotron Radiation Light Source, a user facility at SLAC National Accelerator Laboratory, was supported by the U.S. Department of Energy, Office of Science, Office of Basic Energy Sciences under Contract No. DE-AC02-76SF00515.

References

1 G. Ruzette, P. R. Soo, D. R. Sadoway and A. M. Mayes, Melt-Formable Block Copolymer Electrolytes for Lithium Rechargeable Batteries, *J. Electrochem. Soc.*, 2001, **148**(6), A537–A543.
2 I. Gunkel and T. Thurn-Albrecht, Thermodynamic and Structural Changes in Ion-Containing Symmetric Diblock Copolymers: A Small-Angle X-Ray Scattering Study, *Macromolecules*, 2012, **45**(1), 283–291.
3 W. Young and T. H. Epps, Salt Doping in PEO-Containing Block Copolymers: Counterion and Concentration Effects, *Macromolecules*, 2009, **42**(7), 2672–2678.
4 A. A. Teran and N. P. Balsara, Thermodynamics of Block Copolymers with and without Salt, *J. Phys. Chem. B*, 2014, **118**(1), 4–17.
5 N. S. Wanakule, J. M. Virgili, A. A. Teran, Z. G. Wang and N. P. Balsara, Thermodynamic Properties of Block Copolymer Electrolytes Containing Imidazolium and Lithium Salts, *Macromolecules*, 2010, **43**(19), 8282–8289.

6 G. Jo, H. Ahn and M. J. Park, Simple Route for Tuning the Morphology and Conductivity of Polymer Electrolytes: One End Functional Group Is Enough, *ACS Macro Lett.*, 2013, **2**(11), 990–995.
7 M. T. Irwin, R. J. Hickey, S. Xie, F. S. Bates and T. P. Lodge, Lithium Salt-Induced Microstructure and Ordering in Diblock Copolymer/Homopolymer Blends, *Macromolecules*, 2016, **49**(13), 4839–4849.
8 T. H. Epps, T. S. Bailey, R. Waletzko and F. S. Bates, Phase Behavior and Block Sequence Effects in Lithium Perchlorate-Doped Poly(Isoprene-B-Styrene-B-Ethylene Oxide) and Poly(Styrene-B-Isoprene-B-Ethylene Oxide) Triblock Copolymers, *Macromolecules*, 2003, **36**(8), 2873–2881.
9 I. Nakamura, N. P. Balsara and Z. G. Wang, Thermodynamics of Ion-Containing Polymer Blends and Block Copolymers, *Phys. Rev. Lett.*, 2011, **107**(19), 1–5.
10 C. E. Sing, J. W. Zwanikken and M. O. de la Cruz, Electrostatic Control of Block Copolymer Morphology, *Nat. Mater.*, 2014, **13**, 694–698.
11 V. Ganesan, V. Pyramitsyn, C. Bertoni and M. Shah, Mechanisms Underlying Ion Transport in Lamellar Block Copolymer Membranes, *ACS Macro Lett.*, 2012, **1**(4), 513–518.
12 J. Qin and J. J. de Pablo, Ordering Transition in Salt-Doped Diblock Copolymers, *Macromolecules*, 2016, **49**(9), 3630–3638.
13 S. Naidu, H. Ahn, J. Gong, B. Kim and D. Y. Ryu, Phase Behavior and Ionic Conductivity of Lithium Perchlorate-Doped Polystyrene-B-Poly(2-Vinylpyridine) Copolymer, *Macromolecules*, 2011, **44**(15), 6085–6093.
14 I. Nakamura and Z. G. Wang, Salt-Doped Block Copolymers: Ion Distribution, Domain Spacing and Effective χ Parameter, *Soft Matter*, 2012, **8**(36), 9356.
15 S. Mai, J. P. A. Fairclough, I. W. Hamley, M. W. Matsen, R. C. Denny, B. Liao, C. Booth and A. J. Ryan, Order-Disorder Transition in Poly(Oxyethylene)–Poly(Oxybutylene) Diblock Copolymers, *Macromolecules*, 1996, **29**(19), 6212–6221.
16 J. L. Thelen, A. A. Teran, X. Wang, B. A. Garetz, I. Nakamura, Z. G. Wang and N. P. Balsara, Phase Behavior of a Block Copolymer/Salt Mixture through the Order-to-Disorder Transition, *Macromolecules*, 2014, **47**(8), 2666–2673.
17 I. Nakamura, N. P. Balsara and Z. G. Wang, First-Order Disordered-to-Lamellar Phase Transition in Lithium Salt-Doped Block Copolymers, *ACS Macro Lett.*, 2013, **2**(6), 478–481.
18 M. T. Irwin, R. J. Hickey, S. Xie, S. So, F. S. Bates and T. P. Lodge, Structure-Conductivity Relationships in Ordered and Disordered Salt-Doped Diblock Copolymer/homopolymer Blends, *Macromolecules*, 2016, **49**(18), 6928–6939.
19 P. Medapuram, J. Glaser and D. C. Morse, Universal Phenomenology of Symmetric Diblock Copolymers near the Order-Disorder Transition, *Macromolecules*, 2015, **48**(3), 819–839.
20 I. W. Hamley, M. D. Gehlsen, A. K. Khandpur, K. A. Koppi, J. H. Rosedale, M. F. Schulz, F. S. Bates, K. Almdal and K. Mortensen, Complex Layered Phases Asymmetric Copolymers, *J. Phys. II*, 1994, **4**(12), 2161–2186.
21 A. Karim, N. Singh, M. Sikka, F. S. Bates, W. D. Dozier and G. P. Felcher, Ordering in Asymmetric Poly(Ethylene-propylene)-poly(Ethylethylene) Diblock Copolymer Thin Films, *J. Chem. Phys.*, 1994, **100**(2), 1620.
22 G. Floudas, B. Vazaiou, F. Schipper, R. Ulrich, U. Wiesner, H. Iatrou and N. Hadjichristidis, Poly(ethylene Oxide-B-Isoprene) Diblock Copolymer Phase Diagram, *Macromolecules*, 2001, **34**(9), 2947–2957.
23 T. M. Gillard, S. Lee and F. S. Bates, Dodecagonal Quasicrystalline Order in a Diblock Copolymer Melt, *Proc. Natl. Acad. Sci. U. S. A.*, 2016, **11**(5), 201601692.
24 J. L. Adams, D. J. Quiram, W. Graessley, R. A. Register and G. R. Marchand, Ordering Dynamics of Compositionally Asymmetric Styrene-Isoprene Block Copolymers, *Macromolecules*, 1996, **29**(8), 2929–2938.
25 J. Listak, W. Jakubowski, L. Mueller, A. Plichta, K. Matyjaszewski and M. R. Bockstaller, Effect of Symmetry of Molecular Weight Distribution in Block Copolymers on Formation Of "metastable" morphologies, *Macromolecules*, 2008, **41**(15), 5919–5927.
26 N. Hadjichristidis, H. Iatrou, S. Pispas and M. Pitsikalis, Anionic Polymerization: High Vacuum Techniques, *J. Polym. Sci., Part A: Polym. Chem.*, 2000, **38**(18), 3211–3234.
27 R. Yuan, A. A. Teran, I. Gurevitch, S. A. Mullin, N. S. Wanakule and N. P. Balsara, Ionic Conductivity of Low Molecular Weight Block Copolymer Electrolytes, *Macromolecules*, 2013, **46**(3), 914–921.
28 A. Hexemer, W. Bras, J. Glossinger, E. Schaible, E. Gann, R. Kirian, A. Mac Dowell, M. Church, B. Rude and H. Padmore, A SAXS/WAXS/GISAXS Beamline with Multilayer Monochromator, *J. Phys.: Conf. Ser.*, 2010, **247**, 012007.
29 J. Ilavsky, Nika: Software for Two-Dimensional Data Reduction, *J. Appl. Crystallogr.*, 2012, **45**(2), 324–328.
30 J. R. Kremer, D. N. Mastronarde and J. R. McIntosh, Computer Visualization of Three-Dimensional Image Data Using IMOD, *J. Struct. Biol.*, 1996, **116**(1), 71–76.
31 D. N. Mastronarde, Dual-Axis Tomography: An Approach with Alignment Methods That Preserve Resolution, *J. Struct. Biol.*, 1997, **120**(3), 343–352.
32 D. N. Mastronarde and S. R. Held, Automated Tilt Series Alignment and Tomographic Reconstruction in IMOD, *J. Struct. Biol.*, 2017, **197**(2), 102–113.
33 S. A. Mullin, G. M. Stone, A. A. Teran, D. T. Hallinan, A. Hexemer and N. P. Balsara, Current-Induced Formation of Gradient Crystals in Block Copolymer Electrolytes, *Nano Lett.*, 2012, **12**(1), 464–468.
34 M. Chintapalli, T. N. P. Le, N. R. Venkatesan, N. G. Mackay, A. A. Rojas, J. L. Thelen, X. C. Chen, D. Devaux and N. P. Balsara, Structure and Ionic Conductivity of Polysytrene-*block*-poly(ethylene oxide) Electrolytes in the High Salt Concentration Limit, *Macromolecules*, 2016, **49**(5), 1770–1780.
35 D. M. Pesko, K. Timachova, R. Bhattacharya, M. C. Smith, I. Villaluenga, J. Newman and N. P. Balsara, Negative Transference Numbers in Poly(ethylene oxide)-Based Electrolytes, *J. Electrochem. Soc.*, 2017, **164**(11), E3569–E3575.
36 E. D. Gomez, A. Panday, E. H. Feng, V. Chen, G. M. Stone, A. M. Minor, C. Kisielowski, K. H. Downing, O. Borodin, G. D. Smith and N. P. Balsara, Effect of Ion Distribution on Conductivity of Block Copolymer Electrolytes, *Nano Lett.*, 2009, **9**(3), 1212–1216.

37 J. B. Gilbert, M. Luo, C. K. Shelton, M. F. Rubner, R. E. Cohen and T. H. Epps, Determination of Lithium-Ion Distributions in Nanostructured Block Polymer Electrolyte Thin Films by X-Ray Photoelectron Spectroscopy Depth Profiling, *ACS Nano*, 2015, **9**(1), 512–520.

38 M. A. Webb, Y. Jung, D. M. Pesko, B. M. Savoie, U. Yamamoto, G. W. Coates, N. P. Balsara, Z.-G. Wang and T. F. Miller III, Systematic computational and experimental investigation of lithium-ion transport mechanisms in polyester-based polymer electrolytes, *ACS Cent. Sci.*, 2015, **1**(4), 198–205.

39 F. Müller-Plathe, W. F. Van Gunsteren and F. Mü Ller-Plathe, Computer simulation of a polymer electrolyte: Lithium Iodide in amorphous poly(ethylene oxide), *J. Chem. Phys.*, 1995, **103**(103), 4745–4756.

40 O. Borodin and G. D. Smith, Mechanisms of ion transport in amorphous poly(ethylene oxide)/LiTFSI from molecular dynamics simulations, *Macromolecules*, 2006, **39**(4), 1620–1629.